Pergamon

Int. J. Multiphase Flow Vol. 23, No. 3, pp. 503–522, 1997

Printed in Great Britain
PII: S0301-9322(96)00083-3
0301-9322/97 $17.00 + 0.00

WAVE INDUCED SECONDARY MOTIONS IN STRATIFIED DUCT FLOW

M. NORDSVEEN† and A. F. BERTELSEN

University of Oslo, Department of Mathematics, Section of Mechanics, P.O. Box 1053, Blindern N-0315, Oslo 3, Norway

(Received 16 October 1994; in revised form 30 October 1996)

Abstract—Turbulent gas–liquid stratified flow in near horizontal, straight ducts with a regular two dimensional wavy deformation of the interface has been studied. In this flow regime strong mean secondary currents are observed. By applying the Generalized Lagrangian Mean Theory of Andrews and McIntyre (1978a) it is shown that these secondary velocities in the liquid phase may result from an interaction between wave psuedomomentum per unit mass and mean axial velocity. This interaction takes exactly the same form as the Craik and Leibovich 'vortex forces' (Leibovich 1983) for Langmuir circulation in the oceans, but with wave pseudomomentum per unit mass replacing Stokes drift. For a particular case it is shown that the wave pseudomomentum–mean flow interaction is identical to a wave Reynolds stress formulation. Predictions with a numerical implementation of the developed model compares favourably with the experimental results of Suzanne (1985). © 1997 Elsevier Science Ltd. All rights reserved.

Key Words: stratified duct flow, turbulence, waves, secondary currents, GLM theory, wave pseudomomentum

1. INTRODUCTION

Fully developed turbulent gas–liquid stratified flow in near horizontal ducts is considered. In the stratified flow regime Hanratty and Engen (1957), Akai *et al.* (1977), Suzanne (1985) and others have identified a subregime with quite regular deformation of the interface with 2-dimensional waves or 3-dimensional 'pebbled' structures. Akai *et al.* (1977) found that the auto-correlation function for the interface location was periodic for both two and three dimensional deformations, with less distinct periodicity for the three dimensional structure. Suzanne (1985) reported one narrow peak in the wave-energy spectrum for the two dimensional waves and two peaks for the three dimensional waves, one dominant and a smaller at the double frequency. He also reported variations in the wave amplitudes across the duct with the higher amplitudes close to the lateral walls. Together with this regular wave field, Suzanne (1985) observed strong mean secondary flow which formed a cellular structure with two rolls in the liquid phase and two rolls in the gas phase. Liquid was flowing up near the walls and down in the middle of the duct, and gas was flowing down near the walls and up in the middle.

The purpose of this work is to discuss and model mechanisms generating the secondary flow field in the liquid phase.

At least two sources for generation of such secondary flow could be considered. Turbulence induced secondary flow (Prandtl's secondary flow of second kind) are known to exist in pipes with non-circular cross section. Einstein and Li (1958) showed theoretically for single phase turbulent flow in a straight conduit that anisotropy in the turbulent Reynolds stresses may introduce axial mean vorticity. Naot and Rodi (1982) applied an algebraic Reynolds stress model to predict turbulence generated secondary currents in open channel flow with a free surface not disturbed by waves, and Nezu and Rodi (1985) measured secondary velocities in open channel flow and related these flow to the turbulence. In Naot and Rodi's computations and the measurements of Nezu and Rodi the secondary velocities attain their largest values close to the lateral walls with relatively small values a few liquid heights away from the lateral walls. This coincides with Suzanne's (1985)

†Present address: Institute for Energy Technology, 2007 Kjeller, Norway.

findings of no secondary currents in the middle of the duct when the interface was not disturbed by waves. The distance from the lateral walls to the middle of the duct for Suzanne's case was about 2.5 liquid heights. However, as already mentioned, with the onset of regular waves at the interface, Suzanne (1985) reported strong mean secondary velocities in the middle of the duct with weaker secondary velocities towards the lateral walls. This indicates that the secondary currents could be induced by the wave field. In this work we focus on modelling wave generated secondary flow, and the effect of turbulence is modelled applying a standard k–ϵ model which is known not to be able to predict turbulence generated secondary flow.

There is a resemblance between our case and Langmuir circulations occurring in the oceans. When the wind blows over a water surface and generates waves, numerous streaks parallel to the wind direction may be observed. Langmuir (1938) related these streaks to convergence lines between counter rotating vortices below the surface. Different mechanisms for generating Langmuir circulation have been proposed in the literature. Craik and Leibovich (1976), Craik (1977) and Leibovich (1977) presented models where the vortices are induced by interactions between the wave field related Stokes drift and a weak wind-induced shear flow. These models have been divided into two classes denoted CL1 and CL2. Leibovich (1983) reviewed the subject and discussed the two CL mechanisms in terms of 'vortex forces' in the vorticity equation given by

$$\tilde{\mathbf{S}}_{\mathrm{CL}} = \underbrace{(\tilde{w}^{\mathrm{S}}_{,x} W_{,y}}_{\tilde{S}_{\mathrm{CL1}}} - \underbrace{\tilde{w}^{\mathrm{S}}_{,y} W_{,x})\mathbf{i}_z}_{\tilde{S}_{\mathrm{CL2}}}. \qquad [1]$$

Here $\tilde{w}^{\mathrm{S}}$, W and $\mathbf{i}_z$ denote Stokes drift, mean flow velocity and the unit vector in the wind direction, respectively. x is horizontal coordinate perpendicular to the wind and y is the vertical coordinate. Subscripts $,x$ and $,y$ mean differentiation with respect to x and y.

In the CL1 models, the wave field is composed of two crossing linear waves propagating with equal and opposite angles to the wind direction. This gives a Stokes drift which varies in the x direction. The mean shear flow varies in the y direction and vorticity is produced by a nonzero $\tilde{S}_{\mathrm{CL1}}$ term.

The CL2 models are based on an instability mechanism. A perturbation of the mean shear flow gives a small variation with x. Since the Stokes drift varies with y, a nonzero $\tilde{S}_{\mathrm{CL2}}$ term induces vorticity and cross stream motion which amplifies the perturbation.

An important difference between flow in the ocean and in ducts is the relative magnitude between the mean shear flow and the wave perturbation. In the Craik and Leibovich models the wave field is developed in a perturbation series in the wave steepness $\epsilon_1 \ll 1$. To first order the wave field is given by an irrotational wave solution, with the traditional Stokes drift to second order. The mean shear flow is assumed to be weak of $o(\epsilon_1)$. In duct flow we have a strong shear flow of $O(1)$ giving a rotational wave field of $O(\epsilon_1)$. Nevertheless, Benkirane *et al.* (1990) applied a CL2 model for duct flow and obtained secondary velocities which agreed well with Suzanne's (1985) measurements.

In a model by Nordsveen and Bertelsen (1993) it was assumed that the wave field was composed of two crossing linear wave trains which interacted with a strong mean flow giving a rotational wave solution. An averaging procedure (Reynolds and Hussain 1972) with a decomposition of the flow field f into a mean component F, a wave component $\tilde{f}$ and a turbulent component f' was applied to the Navier–Stokes and continuity equations for incompressible flow. The mean flow momentum equations became

$$\nabla\cdot(\mathbf{V}\mathbf{V}) = -\frac{1}{\rho}\nabla P + \nabla\Phi - \nabla\cdot(\overline{\mathbf{v}'\mathbf{v}'}) - \nabla\cdot(\overline{\tilde{\mathbf{v}}\tilde{\mathbf{v}}}), \qquad [2]$$

where $\mathbf{V}$ is mean velocity, ρ is density, P is mean pressure and $\nabla\Phi$ is the gravity force per unit mass. Turbulent Reynolds stresses per unit mass $\underline{R}' = -\mathbf{v}'\mathbf{v}'$ were modelled with a k–ϵ model while the wave Reynolds stresses per unit mass $\tilde{R} = -\tilde{\mathbf{v}}\tilde{\mathbf{v}}$ were calculated from the simultaneous solution of a momentum equation for the wave field where the mean axial velocity's variation with depth was taken into account. These wave Reynolds stresses became a source for mean secondary flow. However, the predicted secondary flow were small compared with the reported experimental results of Suzanne (1985). In this model there is an interaction between two crossing wave trains and the vertical variation of the mean axial velocity. There is thus some resemblance to the CL1 model.

In an attempt to analyze the strong mean flow case (duct) further, we decided to apply the Generalized Lagrangian Mean (GLM) theory of Andrews and McIntyre (1978a). Leibovich (1980) applied this general theory for wave mean flow interactions to rederive the CL theories. A motivation for adopting the GLM-theory is well expressed by Leibovich (1980): "... the introduction by Leibovich and Ulrich (1972) of the ordering incorporated in the CL theories—an ordering generally in accord with observed motions involving wind-generated waves and currents in the ocean—was an essential step in the derivation of equations describing nonlinear rectified effects of waves on currents by the CL method. By contrast, the GLM equations of AM describe such rectified effects without the need to invoke the CL assumptions, and suggest that some of the essential mathematical structure underlying the existence of Langmuir-circulation instability might carry over into conditions under which the CL equations do not apply: in particular, when wave orbital speeds are not large compared to mean currents (so the waves can no longer be essentially irrotational) ...".

Craik (1982a, 1982b) applied the GLM theory in an investigation of hydrodynamic stability of parallel shear flow. Due to a resemblance to the case studied here, we have been able to utilize some of his results. Magnaudet (1989) made a thorough analysis of wavy stratified duct flow and investigated also the interactions between waves and turbulence. We have not taken such interactions into account in this work.

In section 2 we present the mathematical model and compare it with the model by Nordsveen and Bertelsen (1993) as well as the Craik and Leibovich models. In section 3 the numerical method is presented and in section 4 predictions with the developed model are presented and compared with the experimental results of Suzanne (1985). A discussion of the results and the conclusions are found in section 5.

2. THEORY

A sketch of the flow problem in a near horizontal duct is given in figure 1. A Cartesian coordinate system (x, y, z) is used, where for a horizontal duct, x is the horizontal, spanwise direction, y is the vertical direction and z is the axial direction. The inclination angle of the duct is denoted γ. The bottom of the duct, the mean liquid height and the lateral walls are given by $y = 0$, $y = H_L$ and $x = \pm L_W$, respectively.

We investigate the flow in the liquid which is assumed incompressible and Newtonian under the influence of a constant gravitational field. As briefly reviewed in the introduction, observation on the flow problem considered in this paper, indicate that the flow field may be depicted as being composed of a steady, a periodic and a randomly fluctuating (turbulent) component. The observed (Suzanne 1985) deformation of the interface indicate that the regular interface deformation can be modelled by linear harmonic waves. Waves tend to be linear when

$$\epsilon_1 = \max(a/\lambda, a/H_L) \ll 1 \qquad [3]$$

where a and λ are the amplitude and length of the waves, respectively. The mean secondary velocities are small compared with the mean axial velocity. This means that

$$\epsilon_2 = \max(U/W_B, V/W_B) \ll 1, \qquad [4]$$

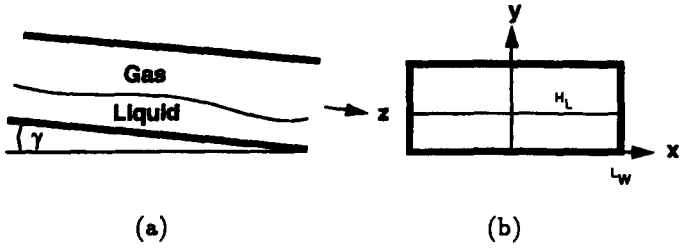

Figure 1. A sketch of the duct flow problem. (a) Axial cut. (b) Cross section.

where U, V denote the mean velocity components in the x and y directions, respectively, and W_B is the bulk velocity.

2.1. Conservation equations

The flow is governed by the following continuity and momentum equations

$$\nabla\cdot\mathbf{v} = 0, \tag{5}$$

$$\mathbf{v}_{,t} + \nabla\cdot(\mathbf{v}\mathbf{v}) = -\frac{1}{\rho}\nabla p + \mathbf{X} + \nabla\Phi. \tag{6}$$

Here $\mathbf{v}$ is velocity, p is pressure, ρ is density, $\nabla\Phi = (0, -g\cos\gamma, g\sin\gamma)$, $\mathbf{X} = \nu\nabla^2\mathbf{v}$, g is acceleration of gravity and ν is molecular, kinematic viscosity. Subscript $,t$ means differentiation with respect to time t.

We will develop the mathematical models along two paths, named the Eulerian and the GLM approach. The Eulerian approach was used by Nordsveen and Bertelsen (1993) while the GLM approach is novel to this work. In the following $f(\mathbf{x}, t)$ will denote different flow field quantities. We use the phase average of Reynolds and Hussain (1972)

$$\langle f(\mathbf{x}, t)\rangle = \lim_{N\to\infty}\frac{1}{N+1}\sum_{n=0}^{N} f(\mathbf{x}, t + n\tau), \tag{7}$$

where τ is the period of the regular wave component, and a time average

$$\bar{f}(\mathbf{x}) = \lim_{T\to\infty}\frac{1}{T}\int_{-T/2}^{T/2} f(\mathbf{x}, t)\mathrm{d}t. \tag{8}$$

Introducing the turbulent component $f' = f - \langle f\rangle$ and phase average [6] gives the phase averaged Navier–Stokes equations (see Reynolds and Hussain 1972)

$$\langle\mathbf{v}\rangle_{,t} + \nabla\cdot(\langle\mathbf{v}\rangle\langle\mathbf{v}\rangle) = -\frac{1}{\rho}\nabla\langle p\rangle + \langle\mathbf{X}\rangle + \nabla\langle\Phi\rangle - \nabla\cdot\langle\mathbf{v}'\mathbf{v}'\rangle. \tag{9}$$

Eulerian approach. The flow field f is decomposed as $f = F + \tilde{f} + f'$, where $F = \bar{f}$ is the mean component, $\tilde{f} = \langle f\rangle - F$ is the wave component and $f' = f - \langle f\rangle$ is the turbulent component. Applying this decomposition and the averages [7] and [8] to the basic equations [5] and [6] give

$$\nabla\cdot\mathbf{V} = 0, \quad \nabla\cdot\tilde{\mathbf{v}} = 0. \tag{10}$$

$$\nabla\cdot(\mathbf{V}\mathbf{V}) = -\frac{1}{\rho}\nabla P + \nabla\Phi - \nabla\cdot\overline{(\mathbf{v}'\mathbf{v}')} - \nabla\cdot(\overline{\tilde{\mathbf{v}}\tilde{\mathbf{v}}}). \tag{11}$$

The flow studied is turbulent and we use wall functions to describe boundary conditions in the (turbulent) log-layer away from the walls. The molecular viscosity term is therefore neglected. The momentum equations contain now both a turbulent and a wave Reynolds stress tensor. To obtain a closed boundary value problem, we will calculate the wave velocity field $\tilde{\mathbf{v}}$ and model the turbulent Reynolds stresses.

The momentum equations for the wave field are obtained as the difference between the phase averaged [9] and the time averaged [11] momentum equations (see Reynolds and Hussain 1972). These equations are simplified applying an order of magnitude analysis where we utilize that $W \sim W_B$, $U \sim V \ll W_B$ and $\tilde{\mathbf{v}} \ll W_B$. The difference between the phase averaged and time averaged turbulent Reynolds stress tensors are also neglected. Molecular viscosity effects are disregarded and we do not take into account the variation in the mean axial velocity across the width of the duct. This last simplification are not valid close to the lateral walls. However, we apply the model only to wide duct flow and the approximation is thus believed to be good over the main part of the

calculation domain. The momentum equations for the wave field read

$$\tilde{\mathbf{v}}_{,t} + \hat{W}\cdot\nabla\tilde{\mathbf{v}} = \tilde{v}\hat{W}_{,y}\mathbf{i}_z + -\frac{1}{\rho}\nabla\tilde{p}, \qquad [12]$$

where $\hat{W}(y) = 1/(2L_w)\int_{-L_w}^{L_w} W(x, y)\mathrm{d}x$, is the average of the axial mean velocity over the width of the duct. The turbulent Reynolds stresses per unit mass are modelled using the generalized Boussinesq hypothesis

$$-\overline{\mathbf{v}'\mathbf{v}'} = \nu_t(\nabla\mathbf{V} + \nabla\mathbf{V}^{\mathrm{T}}) - \frac{2}{3}k\mathscr{I}, \qquad [13]$$

where $\mathscr{I}$ is the unit tensor, k is the turbulent kinetic energy per unit mass and ν_t is the eddy viscosity modelled by the k–ϵ turbulence model $\nu_t = c_\mu k^2/\epsilon$, where ϵ is the dissipation rate of k. We adopt the transport equations for k and ϵ as given by Rodi (1980)

$$\mathbf{V}\cdot\nabla k = \nabla\cdot\left(\frac{\nu_t}{\sigma_k}\nabla k\right) + \underbrace{\nu_t(\nabla\mathbf{V} + \nabla\mathbf{V}^{\mathrm{T}}):\nabla\mathbf{V}}_{P_k} - \epsilon, \qquad [14]$$

$$\mathbf{V}\cdot\nabla\epsilon = \nabla\cdot\left(\frac{\nu_t}{\sigma_\epsilon}\nabla\epsilon\right) + \frac{\epsilon}{k}(c_{1\epsilon}P_k - c_{2\epsilon}\epsilon). \qquad [15]$$

The constants in the turbulence model are given in table 4.

GLM approach. Instead of the more direct procedure for developing the mean Eulerian momentum equations [11], we will now first develop mean Lagrangian momentum equations using the GLM theory of Andrews and McIntyre (1978a). These momentum equations are subsequently converted to mean Eulerian momentum equations.

Central to the GLM description is the mapping $\mathbf{x} \rightarrow \boldsymbol{x} + \boldsymbol{\xi}(\mathbf{x}, t)$, where $\boldsymbol{\xi}(\mathbf{x}, t)$ is a field related to a displacement about the position $\mathbf{x}$. The following notation is introduced $\underline{f^{\xi}(\mathbf{x}, t)} \equiv \underline{f(\mathbf{x} + \boldsymbol{\xi}(\mathbf{x}, t), t)}$, and an exact Lagrangian mean operator $(\,)^{\mathrm{L}}$ is defined by $f(\mathbf{x}, t)^{\mathrm{L}} \equiv f^{\xi}(\mathbf{x}, t)$, where in our case $(\,)$ is the time average [8]. That is, for each $\mathbf{x}$ the average is taken over the positions $\mathbf{x} + \boldsymbol{\xi}(\mathbf{x}, t)$. It is required that $\boldsymbol{\xi}(\mathbf{x}, t) = 0$ implying that $\boldsymbol{\xi}$ is a disturbance quantity. The fluctuation f^{l} in the GLM theory is defined as $f^{\mathrm{l}} = f^{\xi} - \bar{f}^{\mathrm{L}}$ and it follows that $\bar{f}^{\mathrm{l}} = 0$.

The phase averaged momentum equations [9] are now evaluated in the displacement points $\mathbf{x} + \boldsymbol{\xi}$, multiplied by $\mathbf{V}(\mathbf{x} + \boldsymbol{\xi})$ and time averaged using [8]. The displacement $\boldsymbol{\xi}$ is related to the phase averaged field and not the total field. The resulting equations read

$$\bar{D}^{\mathrm{L}}(\bar{\mathbf{v}}^{\mathrm{L}} - \mathbf{P}) + \nabla\bar{\mathbf{v}}^{\mathrm{L}}\cdot(\bar{\mathbf{v}}^{\mathrm{L}} - \mathbf{P}) = -\nabla\pi - \bar{\mathbf{X}}^{\mathrm{L}} - \overline{\nabla\boldsymbol{\xi}\cdot\mathbf{X}^{\mathrm{l}}} - \underbrace{\overline{\nabla(\mathbf{x} + \boldsymbol{\xi})\cdot\nabla\cdot\langle\mathbf{v}'\mathbf{v}'\rangle}}_{\mathrm{IV}} \qquad [16]$$

where $\pi = \bar{p}^{\mathrm{L}}/\rho + \bar{\Phi}^{\mathrm{L}} - \overline{\mathbf{v}^{\xi}\cdot\mathbf{v}^{\xi}}/2$. Comparing with theorem I, section 3, [3.8] in Andrews and McIntyre (1978a), this equation has the additional term IV due to the separation of the total field into a turbulent field and a phase averaged field. $\mathbf{P}$ is the wave pseudomomentum per unit mass, which is given by

$$\mathbf{P} = (P_x, P_y, P_z) = -\overline{\nabla\boldsymbol{\xi}\cdot\mathbf{v}^{\mathrm{l}}}. \qquad [17]$$

Here, $\mathbf{v}^{\mathrm{l}}$ is the fluctuating part of the Lagrangian velocity field, which for small amplitude waves is expressed as $\mathbf{v}^{\mathrm{l}} = \tilde{\mathbf{v}} + \boldsymbol{\xi}\cdot\nabla\mathbf{V} + O(\epsilon_1^2)$. The equations [16] are equations for the Lagrangian mean field. In appendix A these equations are expressed in terms of the Eulerian field assuming small amplitude waves and neglecting interactions between waves and turbulence. We obtain

$$\nabla\cdot(\mathbf{V}\mathbf{V}) = -\nabla\pi - \nabla\cdot\overline{\mathbf{v}'\mathbf{v}'} + \underbrace{\bar{\mathbf{v}}^{\mathrm{S}}\times\nabla\times\mathbf{V} + (\mathbf{V} + \bar{\mathbf{v}}^{\mathrm{S}})\times\nabla\times(\bar{\mathbf{v}}^{\mathrm{S}} - \mathbf{P})}_{\tilde{\mathbf{S}}} \qquad [18]$$

with $\pi = \bar{p}^{\mathrm{L}}/\rho + \bar{\Phi}^{\mathrm{L}} - \bar{\mathbf{V}}\cdot\bar{\mathbf{V}}/2 + \mathbf{V}\cdot(\bar{\mathbf{v}}^{\mathrm{S}} - \mathbf{P})$. $\bar{\mathbf{v}}^{\mathrm{S}}$ is the Stokes drift which is defined as the difference

between the mean Lagrangian and the mean Eulerian velocity. It should be noted that the assumption of small amplitude waves is only used to simplify the expression for π and the turbulent Reynolds stress tensor. The wave field mean flow interaction term $\tilde{\mathbf{S}}$ is also valid for large amplitude waves. For an order ϵ_1 disturbance ξ (small amplitude waves) the Stokes drift can be expressed as

$$\bar{\mathbf{v}}^S = \overline{\boldsymbol{\xi}\cdot\nabla\tilde{\mathbf{v}}} + \frac{1}{2}\overline{\boldsymbol{\xi}\boldsymbol{\xi}}:\nabla\nabla\mathbf{V} + O(\epsilon_1^3). \tag{19}$$

For a weak Eulerian mean shear flow of $o(\epsilon_1)$ disturbed by a linear irrotational wave field of $O(\epsilon_1)$, Andrews and McIntyre (1978a) showed [6.9] that $\mathbf{P} = \bar{\mathbf{v}}^S + O(\epsilon_1^3)$. In that case the $\tilde{S}$-term in [18] simplifies to the Craik and Leibovich source for Langmuir circulation

$$\tilde{\mathbf{S}}_{CL} = \bar{\mathbf{v}}^S \times \nabla \times \mathbf{V}. \tag{20}$$

For waves on strong mean shear flow of $O(1)$ $\mathbf{P} \neq \bar{\mathbf{v}}^S$. The terms $\tilde{S}$ and π are simplified applying an order of magnitude analysis where we utilize that $W \sim W_B$, $U \sim V \ll W_B$, $\tilde{\mathbf{v}} \ll W_B$ and assume that $P_x \sim P_y \ll P_z$ and $\bar{u}^S \sim \bar{v}^S \ll \bar{w}^S$. For the wave field model used in this work $P_x = P_y = 0$ and $\bar{u}^S = \bar{v}^S = 0$. The momentum equations [18] are now given by

$$\nabla\cdot(\mathbf{VV}) = -\nabla\pi - \nabla\cdot\overline{\mathbf{v}'\mathbf{v}'} + \underbrace{P_z W_{,y}\mathbf{i}_y}_{\tilde{S}_1} + \underbrace{P_z W_{,x}\mathbf{i}_x}_{\tilde{S}_2}, \tag{21}$$

where $\pi = \bar{p}^L/\rho + \bar{\Phi}^L - \overline{\tilde{\mathbf{v}}\cdot\tilde{\mathbf{v}}}/2$. The equations [21] are the mean momentum equations used in this work. The turbulent Reynolds stresses are modelled as in [13]–[15]. The wave field is given by the solution of the momentum equations [12] and the continuity equation [10].

Taking the curl of equation [21] we obtain the vorticity equation

$$\nabla\times\nabla\cdot(\mathbf{VV}) = -\nabla\times\nabla\cdot\overline{\mathbf{v}'\mathbf{v}'} + \underbrace{(P_{z,x}W_{,y}}_{\tilde{S}_{\Omega 1}} - \underbrace{P_{z,y}W_{,x})\mathbf{i}_z}_{\tilde{S}_{\Omega 2}}. \tag{22}$$

Comparing with the Craik and Leibovich 'vortex forces' [1], we see that wave pseudomomentum per unit mass replaces Stokes drift in the source for axial vorticity.

2.2. *Boundary conditions*

We assume linear waves and prescribe boundary conditions at the mean interface. The validity of this approach is discussed in section 2.3.

The wave field. The applied boundary conditions for the wave field are

$$\eta_{,t} + \hat{W}\eta_{,z} = \tilde{v} \quad ,y = H_L, \tag{23}$$

$$\tilde{p} - \rho g\eta = 0 \quad ,y = H_L, \tag{24}$$

$$\tilde{v} = 0 \quad ,y = 0, \tag{25}$$

$$\tilde{u} = 0 \quad ,x = \pm L_W. \tag{26}$$

Suzanne (1985) reported a variation of the wave amplitude across the width of the duct with about a doubling of the amplitude from the center towards the lateral walls. Magnaudet (1989) related this to the lateral variation in the axial velocity with the occurrence of caustics focussing the wave energy. However, this lateral variation in the mean axial velocity is not taken into account in our wave field momentum equation.

We have used two models for the interface deformation η. In *the interfacial model A* the interface is deformed by two crossing wave trains propagating with equal and opposite angle to the axial direction. This gives

$$\eta = 2a \sin\beta x \sin[\alpha(z - ct)], \tag{27}$$

where a is the amplitude of each wave, β and α are wave numbers and c is the wave speed. A

corresponding wave velocity field obeying the boundary conditions, the wave continuity and momentum equation is given by

$$\tilde{u} = 2\phi_x(y)\cos\beta x \cos[\alpha(z - ct)], \quad [28]$$

$$\tilde{v} = 2\phi_y(y)\sin\beta x \cos[\alpha(z - ct)], \quad [29]$$

$$\tilde{w} = 2\phi_z(y)\sin\beta x \sin[\alpha(z - ct)], \quad [30]$$

with $\beta = \pi/(2L_W)$. ϕ_y is given by Rayleigh's stability equation

$$(\hat{W} - c)(\phi_{y,yy} - k_w^2\phi_y) - \phi_y\hat{W}_{,yy} = 0, \quad [31]$$

where $k_w = \sqrt{\alpha^2 + \beta^2}$ is the wave number. This equation subject to boundary conditions obtained from [23]–[25] is solved numerically. $\phi_x(y)$ and $\phi_z(y)$ are expressed in terms of $\phi_y(y)$ as

$$\phi_x(y) = \frac{\beta}{k_w^2}\left(\phi_{y,y} - \frac{\phi_y\hat{W}_{,y}}{\hat{W} - c}\right), \quad [32]$$

$$\phi_z(y) = -\frac{\alpha}{k_w^2}\left(\phi_{y,y} + \frac{\beta^2}{\alpha^2}\frac{\phi_y\hat{W}_{,y}}{\hat{W} - c}\right). \quad [33]$$

In this first model for the interface deformation, the wave amplitude variation is overestimated.

In *the interfacial model B* the interface is deformed by one wave train propagating in the axial direction giving no wave amplitude variation. The interface deviation and corresponding velocities are given by

$$\eta = 2a\sin[k_w(z - ct)] \quad [34]$$

$$\tilde{u} = 0, \quad [35]$$

$$\tilde{v} = \phi_y(y)\cos[k_w(z - ct)], \quad [36]$$

$$\tilde{w} = -\frac{\phi_{y,y}}{k_w}\sin[k_w(z - ct)]. \quad [37]$$

ϕ_y is once more obtained from the solution of Rayleigh's stability equation.

The mean field. In solving the equation set, a long section of the duct is regarded. A unidirectional uniform mean velocity field as well as a uniform turbulent field are specified as inlet conditions. The length of the duct is adjusted entailing a fully developed flow field at the outlet of the duct. Symmetry conditions are applied for the mean flow field at the middle of the duct $x = 0$. At the bottom and lateral walls the wall shear stress τ_w is found from inverting the logarithmic wall function for the tangential velocity component $U_T = u_\tau \ln(Ey^+)/\kappa$, where $u_\tau = \sqrt{\tau_w/\rho}$ is the friction velocity, $y^+ = yu_\tau/\nu$ is a dimensionless wall distance, y is the distance from the wall, $\kappa = 0.42$ and $E = 9.0$. The wall shear stress (decomposed into the Cartesian directions) becomes the boundary condition for the velocity components parallel to the walls. The velocity component normal to the walls is set to zero. k and ϵ are specified in the logarithmic wall layer by $k = u_\tau^2/\sqrt{c_\mu}$ and $\epsilon = u_\tau^3/(\kappa y)$. At the mean interface a zero stress condition $U_{,y} = 0$ apply for the U velocity component. For the V velocity component a zero mean momentum flux normal to the mean interface is specified. The boundary condition for the W velocity component at the mean interface is prescribed by the interfacial shear stress $\tau_i(x)$ condition

$$\tau_i(x) = \tau_i(0)\left(\frac{L_W - x}{L_W}\right)^{1/4} \quad ,y = H_L, \quad [38]$$

developed by Nordsveen and Bertelsen (1993). The value $\tau_i(0)$ is taken from experiments. The

Table 1. Linearization and Taylor series expansion criteria for the interfacial boundary conditions

$a/H_L \ll 1$	$a/\lambda \ll 1$	$a/\delta_1 \ll 1$	$a/\delta_2 \ll 1$

Table 2. Values of the above criteria where experimental data of Suzanne (1985) and molecular viscosity are used

$a/H_L \sim 0.04$	$a/\lambda \sim 0.017$	$a/\delta_1 \sim 6.3$	$a/\delta_2 \sim 0.6$

boundary condition [38] models the decrease in the interfacial shear stress towards the lateral walls. The interfacial boundary conditions used for k and ϵ are

$$k_{,y} = 0 \quad ,y = H_L, \tag{39}$$

$$\epsilon = k^{3/2}/(0.18H_L) \quad ,y = H_L. \tag{40}$$

These interfacial conditions for k and ϵ were used by Celik and Rodi (1984) for turbulent open channel flow and the boundary condition for ϵ was chosen to obtain the correct decrease in eddy viscosity towards the interface. A zero gradient condition for ϵ, together with the k–ϵ turbulence model used here was found to give the maximum eddy viscosity at the interface.

2.3. *Validation of the interfacial description*

In the above presented model boundary conditions for the mean and wave field are prescribed at the mean interface $y = H_L$. Some remarks about the validity of this approach are appropriate. The usual conditions for Taylor series expansion and linearization of the free surface boundary conditions about a mean free surface are $a/\lambda \ll 1$ and $a/H_L \ll 1$ ($\epsilon_1 \ll 1$). Longuet-Higgins (1953) pointed out the existence of a viscous oscillatory boundary layer at a free surface disturbed by waves. The thickness of this layer is approximately given by $\delta_1 = (2\nu/\omega)^{1/2}$, where ω is the wave frequency. The corresponding condition for the Taylor series expansion and linearization about the mean surface is $a/\delta_1 \ll 1$. In our case we also have a mean boundary layer δ_2 at the interface due to the mean shear stress from the gas. The phase averaged interface is given by $y = H_L + \eta$. Turbulent fluctuations at the interface are ignored and we Taylor series expand the kinematic interfacial boundary condition for the wave field about the mean interface and neglect all nonlinear terms but one. The condition then reads

$$\eta_{,t} + (\hat{W} + \eta \hat{W}_{,y})\eta_{,z} = \hat{v}. \tag{41}$$

The nonlinear term can be neglected if $a\hat{W}_{,y}/\hat{W} = a/\delta_2 \ll 1$ with $\delta_2 = \hat{W}/\hat{W}_{,y}$. The second boundary layer can be stipulated using the relation $\tau_i/\rho = (\nu_t)\hat{W}_{,y}$ at the interface with $\nu_t = 1.0 \times 10^{-6}$ m^2/s, the molecular viscosity. This gives a minimum thickness of δ_2, since some turbulence will remain even at the interface entailing a larger eddy viscosity.

It is now interesting to check the linearization criteria, listed in table 1, applying physical data listed in table 3. Molecular viscosity is used to calculate both δ_1 and δ_2. The result is presented in table 2. The third criterion in the table 1 is hardly fulfilled while the last criterion possibly is, depending on the eddy viscosity.

The conclusion is that the separation into a mean, a wave and a turbulent field with boundary conditions prescribed at the mean interface cannot capture the effect of the oscillatory boundary layer δ_1 in Suzanne's experiments (1985), but the thicker possible more important mean flow boundary layer δ_2, can be modelled. This is reflected in our momentum equation for the wave field where viscous effects are neglected.

Table 3. Experimental data of Suzanne (1985)

$\tau_i/\rho \sim 0.000256$ m^2/s^2	$\hat{W}_{int} \sim 0.5$ m/s	$a \sim 0.0017$ m	$H_L \sim 0.03$ m	$\lambda \sim 0.1$ m	$\omega \sim 55$ Hz

2.4. Comparison between the Eulerian and the GLM approach

We will no compare the Eulerian approach used by Nordsveen and Bertelsen (1993) and the GLM approach used in this work. In the two mean momentum equations [11] and [21], the possible wave field source for mean secondary velocities is represented with the wave Reynolds stress tensor and the wave pseudomomentum term $\tilde{\mathbf{S}} = \tilde{S}_1\mathbf{i}_y + \tilde{S}_2\mathbf{i}_x$, respectively. Taking the curl of these equations, developing the vorticity equation, the gradient terms disappear and it follows that

$$\nabla \times [-\nabla\cdot(\overline{\tilde{\mathbf{v}}\tilde{\mathbf{v}}})] = (\underbrace{P_{z,x}W_{,y}}_{\tilde{S}_{\Omega 1}} - \underbrace{P_{z,y}W_{,x}}_{\tilde{S}_{\Omega 2}})\mathbf{i}_z. \tag{42}$$

We will verify this equality for the wave field given by [23]–[33] which is based on a W-velocity averaged over the width of the duct. The equality [42] is then reduced to

$$\nabla \times [-\nabla\cdot(\overline{\tilde{\mathbf{v}}\tilde{\mathbf{v}}})] = \underbrace{P_{z,x}\hat{W}_{,y}\mathbf{i}_z}_{\tilde{S}_{\Omega 1a}}. \tag{43}$$

The displacement field $\boldsymbol{\xi}$, needed to calculate $\mathbf{P}$, is developed in appendix B and reads

$$\xi_x = \frac{2\phi_x(y)\cos\beta x}{\alpha(\hat{W}-c)}\sin[\alpha(z-ct)] \tag{44}$$

$$\xi_y = \frac{2\phi_y(y)\sin\beta x}{\alpha(\hat{W}-c)}\sin[\alpha(z-ct)] \tag{45}$$

$$\xi_z = \frac{-2\sin\beta x}{\alpha(\hat{W}-c)}\left(\frac{\hat{W}_{,y}\phi_y(y)}{\alpha(\hat{W}-c)} + \phi_z(y)\right)\cos[\alpha(z-ct)]. \tag{46}$$

From the wave field velocities, the displacements and the mean axial velocity, it follows that $P_x = P_y = 0$ and the axial component P_z and $\tilde{S}_{\Omega 1a}$ become

$$P_z = -2\left(\frac{\sin^2\beta x}{\hat{W}-c}\right)\left[\frac{\alpha^2-\beta^2}{\beta^2}\phi_x^2 + \phi_y^2\right] - \frac{2\phi_x^2}{\hat{W}-c}, \tag{47}$$

$$\hat{S}_{\Omega 1a} = -2\beta\sin(2\beta x)\left(\frac{\hat{W}_{,y}}{\hat{W}-c}\right)\left[\frac{\alpha^2-\beta^2}{\beta^2}\phi_x^2 + \phi_y^2\right]. \tag{48}$$

Inserting the wave field velocity components [28]–[30] in the left hand side of [43] the identical expression is obtained. The source [48] was the one used by Nordsveen and Bertelsen (1993).

With the GLM approach the secondary velocity source is expressed as a product of wave pseudomomentum per unit mass and mean axial velocity. This means that even though the transversal mean shear is disregarded in calculating the wave field (and pseudomomentum), it can be taken into account in the source term. Doing this we model the effect of both the $\tilde{S}_{\Omega 1}$ and $\tilde{S}_{\Omega 2}$ terms.

2.5. Stokes drift

Andrews and McIntyre's generalized Stokes drift follows from the Stokes correction equation [19] and is given by

$$\bar{\mathbf{v}}^S = \underbrace{\overline{\boldsymbol{\xi}\cdot\nabla\tilde{\mathbf{v}}}}_{\bar{\mathbf{v}}_1^S} + \underbrace{\frac{1}{2}\overline{\boldsymbol{\xi}\boldsymbol{\xi}}:\nabla\nabla\mathbf{V}}_{\bar{\mathbf{v}}_2^S} + O(\epsilon_1^3). \tag{49}$$

The term $\bar{\mathbf{v}}_1^S$ is the original Stokes drift term and $\bar{\mathbf{v}}_2^S$ is an additional term due to the curvature of

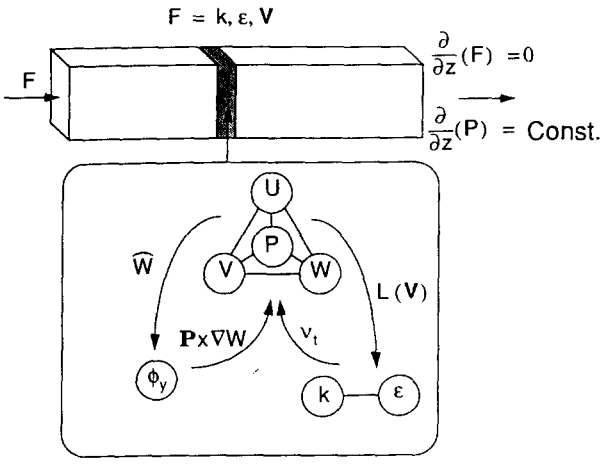

Figure 2. Sketch of solution procedure.

the mean $O(1)$ velocity field. Introducing wave field velocities and disturbance field for crossing waves and the mean axial velocity in [49], it follows that $\bar{u}^S = \bar{v}^S = 0$ and

$$\bar{w}^S = B_1 \cos^2\beta_x - B_2 \sin^2\beta x, \qquad [50]$$

where

$$B_1 = \frac{2\beta\phi_x\phi_z}{\alpha(\hat{W} - c)}$$

$$B_2 = \frac{2\alpha^2\phi_x}{\beta k_w^2(\hat{W} - c)}\left[\phi_{y,y} + \left(2\frac{\beta^2}{\alpha^2} + \frac{\beta^4}{\alpha^4}\right)\frac{\phi_y\hat{W}_{,y}}{\hat{W} - c}\right] + \frac{2\phi_y^2}{\hat{W} - c} + \frac{\phi_y^2\hat{W}_{,yy}}{\alpha^2(\hat{W} - c)^2}.$$

3. NUMERICAL METHOD

The general purpose computer code PHOENICS (Rosten and Spalding 1987) has been adjusted to solve our boundary value problem. In PHOENICS a Cartesian, staggered grid is adopted, and a control volume method is applied to develop finite difference equations which are solved in an efficient forward marching solution procedure. That is, the equations are parabolized in the axial direction and two dimensional equation systems are solved over the cross section, starting at the inlet of the duct with prescribed boundary conditions, marching downstream until a fully developed state is obtained. See figure 2.

4. PREDICTIONS

Predictions with three different models have been performed. In models 1 and 2 we used the interfacial model A with crossing waves. In model 1 only the $\tilde{S}_1$ source in [21] was taken into account. From the analysis in section 2.4, model 1 is the GLM counterpart of the model developed by Nordsveen and Bertelsen (1993). In model 2 both the $\tilde{S}_1$ and the $\tilde{S}_2$ sources were taken into account. In model 3 we used the interfacial model B, with a wave train propagating in the axial

Table 4. Constants in turbulence model

$c_\mu = 0.09$	$\sigma_k = 1.0$	$\sigma_\varepsilon = 1.3$	$c_{1\varepsilon} = 1.44$	$c_{2\varepsilon} = 1.92$

Table 5. Constants in wave model

$a = 0.0012$ m	$\alpha = 62.83\ \text{m}^{-1}$	$\beta = \pi/(2L_W)$	$k_w = 64.77\ \text{m}^{-1}$

Table 6. Other model parameters

$H_L = 0.0315$ m	$L_W = 0.1$ m	$\tau_i(0) = 0.256$ N/m^2	$W_B = 0.476$ m/s

direction. With this interface description only the $\tilde{S}_2$ source is nonzero. The model parameters are as given in tables 4–6.

4.1. *Wave field*

We compare our rotational wave field solution with an irrotational wave field for two crossing wave trains. The irrotational wave field is the solution of the Laplace equation with the same boundary conditions as applied for the rotational wave field. The solid line in figure 3(a) represent the mean axial velocity averaged across the width of the duct. The rotational wave field is based upon this velocity distribution. The dotted line in figure 3(a) represent the cross section averaged mean axial velocity W_B.

In figure 3(b) we have plotted wave pseudomomentum per unit mass and Stokes drift at the lateral walls where they obtain their largest values. The solid and dashed lines is respectively the wave pseudomomentum and generalized Stokes drift for the rotational wave field, while the dotted line is the wave pseudomomentum and Stokes drift for the irrotational wave solution, which to second order in ϵ_1 are identical. The generalized Stokes drift attains negative values close to the interface and is significantly different from the Stokes drift based on the irrotational wave field. Wave pseudomomentum is quite similar for the two wave fields. Since in the duct flow problem it is pseudomomentum which enters the source for secondary velocities, it follows that these sources is qualitatively similar to Craik and Leibovich sources for Langmuir circulations where Stokes drift based on an irrotational wave field is used. This support the findings of Benkirane *et al.* (1990) who applied a CL2 model to predict secondary velocities comparing well with the duct flow measurements of Suzanne (1985).

The amplitude of the wave field velocity components, given by $2\phi_x$, $2\phi_y$ and $2\phi_z$ in [28]–[30], are plotted in figure 4. Here the solid lines represent the rotational wave field and the dotted lines gives the irrotational wave field. Most noticeable is the decrease in the amplitude of the axial wave velocity $2\phi_z$ towards the interface for the rotational wave field. This is caused by the increase of the mean axial velocity towards the interface, as seen in figure 3(a), and is an effect of the mean boundary layer δ_2. The wave speed c is predicted to be 0.883 m/s while Suzanne (1985) measured $c = 0.88$ m/s in the central part of the duct. The maximum axial velocity $\hat{W}$ is about 0.6 m/s giving $c > \max(\hat{W})$ which implies that there is no critical layer present. This is important since the validity of the mapping in the GLM theory fails with the presence of a critical layer.

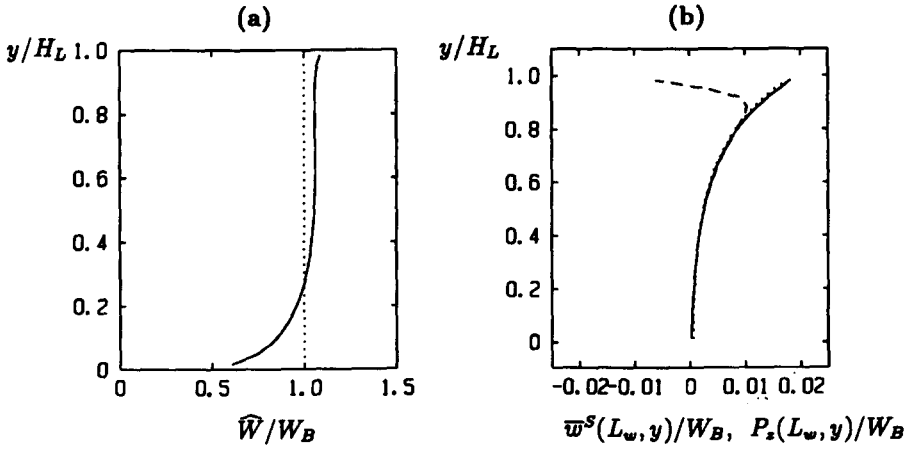

Figure 3. (a) Averaged axial mean velocity. (b) Stokes drift and wave pseudomomentum at lateral wall for crossing wave trains. Dotted line is Stokes drift and wave pseudomomentum for irrotational waves. Dashed and solid lines are Stokes drift and wave pseudomomentum for rotational waves, respectively.

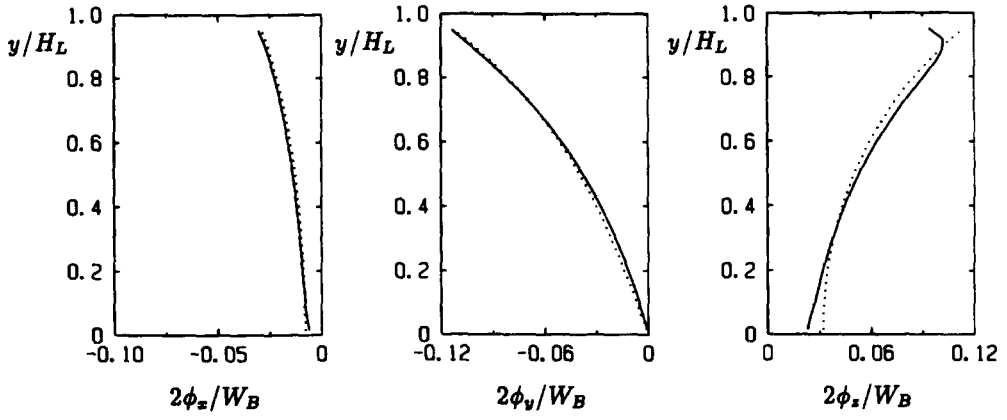

Figure 4. Amplitude of wave field velocity components for crossing wave trains. Rotational solution—solid line. Irrotational solution—dotted line.

4.2. *Mean axial vorticity sources*

The vorticity source $\tilde{S}_{\Omega 1}$ and $\tilde{S}_{\Omega 2}$ for crossing waves (rotational) are shown in figures 5 and 6, respectively. In figure 7, $\tilde{S}_{\Omega 2}$ for the wave field used in model 3 is plotted. In model 1 and model 2 the wave amplitude in the middle of the duct is zero. In model 3 the amplitude is the same all over the width of the duct. Suzanne (1985) reported about a doubling of the amplitude from the middle towards the lateral walls. We chosen the amplitude $2a$ to be less than the measured value close to the lateral walls and larger than the measured amplitude in the middle of the duct. It follows that $\tilde{S}_{\Omega 2}$ in the central part of the duct is underestimated in figure 6 and overestimated in figure 7. Close to the lateral walls $\tilde{S}_{\Omega 2}$ is underestimated for both models 2 and 3. It is seen that $\tilde{S}_{\Omega 2}$ is

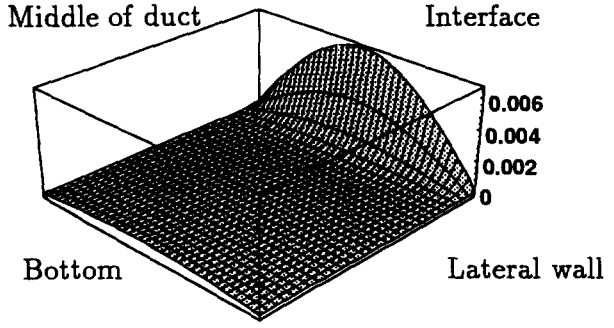

Figure 5. The vorticity source $\tilde{S}_{\Omega 1}$ $(H_L/W_B)^2$, crossing waves.

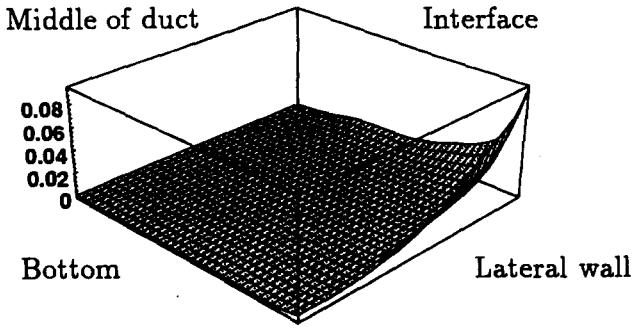

Figure 6. The vorticity source $\tilde{S}_{\Omega 2}$ $(H_L/W_B)^2$, crossing waves.

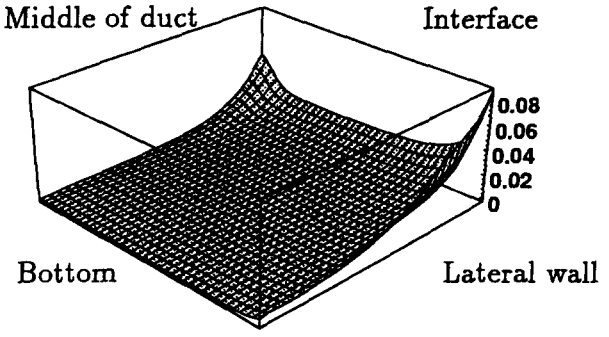

Figure 7. The vorticity source $\tilde{S}_{\Omega 2}$ $(H_L/W_B)^2$, model 3.

up to one order of magnitude larger than $\tilde{S}_{\Omega 1}$. Utilizing that $\max(\sin \beta x \cos \beta x) = 1/2$ and that the wave field decrease exponentially (approximately) with depth we have

$$\max(\tilde{S}_{\Omega 1}) = \max(P_{z,x} W_{,y}) \sim \max(\beta P_z W_{,y}) \quad [51]$$

$$\max(\tilde{S}_{\Omega 2}) = \max(P_{z,y} W_{,x}) \sim \max(2k_w P_z W_{,x}). \quad [52]$$

For the case simulated $\beta \sim 16$ and $k_w \sim 64$ giving that

$$\max(P_{z,y}) \sim 8\max(P_{z,x}). \quad [53]$$

Away from the lateral walls $W_{,y}$ is larger than $W_{,x}$ due to the imposed shear stress from the gas while close to the lateral walls $W_{,x}$ is slightly larger than $W_{,y}$. We conclude that the large difference in the two sources is mainly caused by a larger gradient of wave pseudomomentum with depth than in the spanwise direction. With considerable longer wave lengths in the axial direction and the same wave length in the spanwise direction we would, with the proposed model, obtain $\tilde{S}_{\Omega 1} \sim \tilde{S}_{\Omega 2}$ or even $\tilde{S}_{\Omega 1} > \tilde{S}_{\Omega 2}$. However, to our knowledge, such flow conditions (very long waves—secondary flow) have not been reported in the literature.

4.3. Mean secondary velocities

In figure 8 vector plots of the secondary motions are presented over half the cross section. In figure 9 predicted vertical velocities are compared with experimental results of Suzanne (1985) for three different verticals. All three models predicts secondary velocities flowing up at the walls and down in the middle of the duct. Model 1 fails to reproduce the observed strength of the secondary velocities. This indicates that the interaction between the lateral variation of the wave field and the vertical variation of the mean axial velocity are not the cause for the strong mean secondary

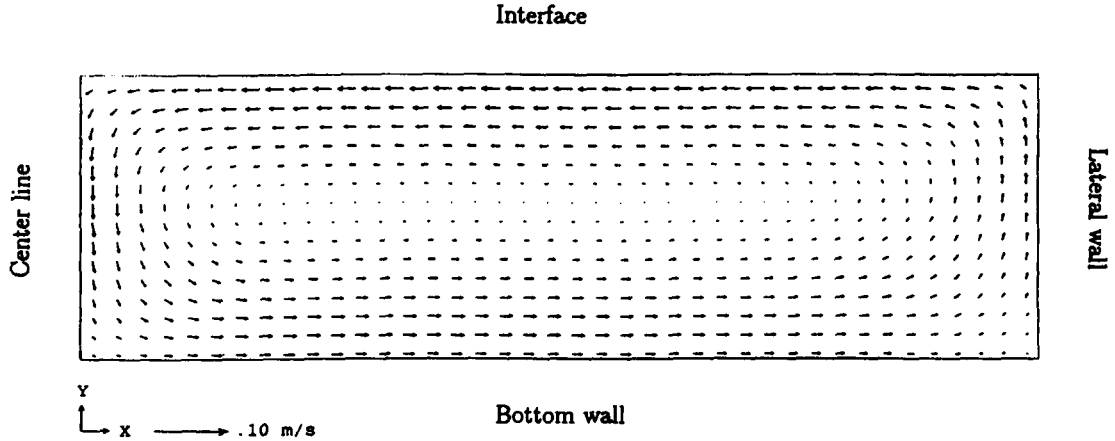

Figure 8. Secondary velocity field.

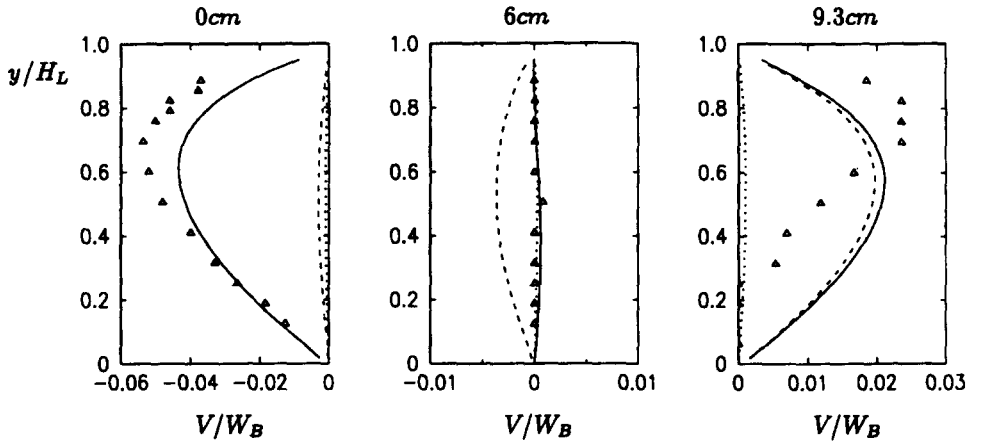

Figure 9. Vertical mean velocity 0, 6 and 9.3 cm from the middle of the duct. Triangles represent experimental results of Suzanne (1985). Lines represent simulations. Dotted line—model 1, dashed line—model 2, solid line—model 3.

velocities. Model 2 predict velocities with the correct magnitude at the walls, but not in the middle of the duct, while model 3 reproduce secondary velocities of correct magnitude at all three verticals. The interaction between the vertical variation of the wave field and the lateral variation of the mean axial velocity gives mean secondary velocities of correct magnitude. As discussed above the mean axial vorticity source (secondary velocities) is underestimated in the middle of the duct in model 2. Close to the lateral wall, figure 9(c), the predictions shows a different behavior than the experiments with higher values close to the bottom. This may be due to the neglect of the horizontal shear flow when calculating the wave field. Especially close to the lateral walls the shear is large with a possible important influence on the wave field. Another limitation in our model is the neglect of turbulence generated secondary velocities known to exist in corners.

4.4. *Mean axial velocity*

In figure 10 predictions and experimental results (Suzanne 1985) of mean axial velocities are shown. Again best agreement between predictions and experiments are obtained for model 3. However, the axial velocity is overpredicted in the middle of the duct and underpredicted close to the lateral wall. This underprediction of lateral mixing can be caused by both slightly too small secondary velocities and too small eddy viscosity.

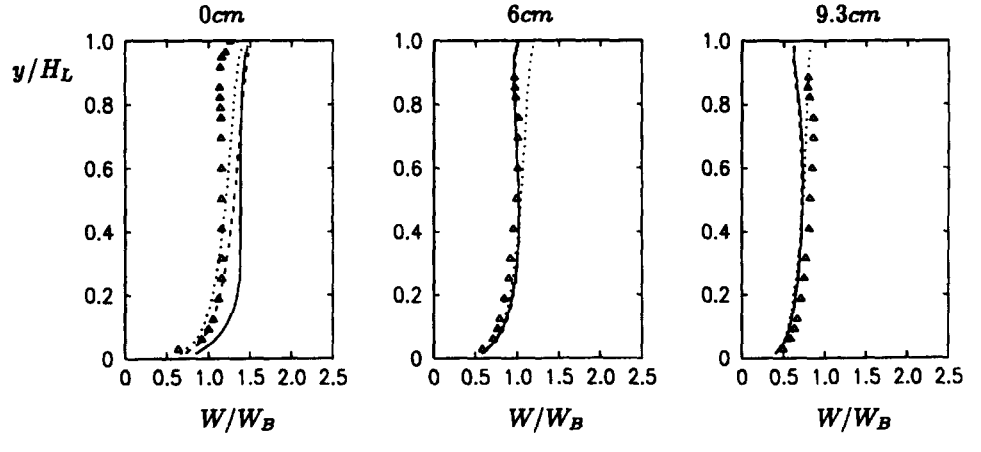

Figure 10. Axial mean velocity 0, 6 and 9.3 cm from the middle of the duct. Triangles represent experimental results of Suzanne (1985). Lines represent simulations. Dotted line—model 1, dashed line—model 2, solid line—model 3.

5. DISCUSSION AND CONCLUSION

In this paper mechanism for generating secondary velocities in regular wavy stratified duct flow has been analyzed. The flow field was decomposed in mean, regular linear wave and irregular turbulent components. In ducts the mean shear flow is of $O(1)$, and the linear wave field of $O(\epsilon_1)$ becomes rotational. The Generalized Lagrangian Mean (GLM) theory of Andrews and McIntyre (1978a) was used to develop an expression for the wave-mean flow interaction. For a particular case it was shown that the GLM formulation is identical to an Eulerian approach with wave Reynolds tensor formalism. However, the interpretation of the wave-mean flow interaction is significantly different in the two approaches. In the Eulerian approach the wave Reynolds tensor is given the interpretation of stresses acting upon the mean flow in such a way that mean secondary velocities are induced. In the GLM approach secondary velocities result from an interaction between wave pseudomomentum per unit mass and mean velocity.

The direct interactions between waves and turbulence are disregarded. A discussion of the oscillatory boundary layer at the interface indicate that including such effects cannot be done with prescribed boundary conditions at a mean interface as used in this work. This was also concluded by Magnaudet (1989) who proposed to solve phase averaged momentum equations in curvilinear coordinates avoiding Taylor series expansions about a mean interface.

We have compared our model for duct flow with Craik and Leibovich (1976, 1977) CL models for Langmuir circulation in the oceans. In the CL models, an $O(\epsilon_1^2)$ Stokes drift (based on a linear $O(\epsilon_1)$ irrotational wave field) interacts with a weak mean flow of $o(\epsilon_1)$ and generates secondary flow. In the above models the mechanisms are exactly the same in duct flow as in the ocean, but with wave pseudomomentum per unit mass replacing Stokes drift. It is then interesting to note that for the irrotational wave field applied in the CL models, Stokes drift and wave pseudomomentum are identical to $O(\epsilon_1^2)$. Our numerical predictions shows that for our rotational wave field applied in ducts the generalized Stokes drift and wave pseudomomentum are significantly different. However, wave pseudomomentum for the irrotational and the rotational wave field are quite similar. This support the findings of Benkirane *et al.* (1990) who applied a CL2 model with irrotational wave field to predict secondary velocities comparing well with the duct flow measurements of Suzanne (1985).

In solving the coupled equation system the horizontal gradient in the mean axial velocity is disregarded in calculating the wave field, but taken into account in the source $\tilde{\mathbf{S}} = \tilde{S}_1\mathbf{i}_y + \tilde{S}_2\mathbf{i}_x$ in [21] generating the secondary velocities. The predicted flow field compared favorably with the experimental results of Suzanne (1985). We discussed the different mechanisms for generating secondary velocities in terms of mean axial vorticity sources [42] and observed that the $\tilde{S}_{\Omega_2}$ source was up to one order of magnitude larger than the $\tilde{S}_{\Omega_1}$ source. That is, the secondary velocities is mainly generated through an interaction between the lateral gradient in the mean axial velocity and the decrease width depth of wave pseudomomentum.

With the wave field used the gradients of pseudomomentum is about 8 times larger in depth than in the spanwise direction. The spanwise gradient of the mean axial velocity close to the lateral walls become of the same order of magnitude as the vertical gradient of the axial velocity close to the interface. In combination this gives a $\tilde{S}_{\Omega_2}$ source larger than $\tilde{S}_{\Omega_1}$. It is worth to note that with considerable longer wave lengths in the axial direction and the same wave length in the spanwise direction we would, with the proposed model, obtain $\tilde{S}_{\Omega_1} \sim \tilde{S}_{\Omega_2}$. We have, however, no evidence for the existence of such a flow field.

A limitation in our implementation is the neglect of the spanwise variation in the mean axial velocity when calculating the wave field (and the pseudomomentum). The horizontal gradient of the axial velocity is large close to the lateral walls and an improvement at this point could be considered. This is especially so since the comparisons between our predictions and Suzanne's experiments showed the largest discrepancy close to the lateral walls. However, near the lateral walls one also expect turbulence induced secondary velocities. The k–ϵ turbulence model used in this work is not capable to predict this and the discrepancy could therefore partly be caused by the applied turbulence model.

REFERENCES

Akai, M., Inoue, A. and Aoki, S. (1977) Structure of a co-current stratified two-phase flow with wavy interphase. *Theo. Appl. Mech.* **25,** 445–455.

Andrews, D. G. and McIntyre, M. E. (1978) An exact theory of nonlinear waves on a Lagrangian-mean flow. *J. Fluid Mech.* **89,** 609–646.

Andrews, D. G. and McIntyre, M. E. (1978) On wave-action and its relatives. *J. Fluid Mech.* **89,** 647–664.

Benkirane, R., Line, A. and Masbernat, L. (1990) Modelling of wavy stratified flow in a rectangular channel. In *ICHMT International Seminar on Phase–Interface Phenomena in Multiphase Flow*, Dubrovnik, 14–18 May 1990.

Craik, A. D. D. and Leibovich, S. (1976) A rational model for Langmuir circulations. *J. Fluid. Mech.* **73,** 401–426.

Craik, A. D. D. (1977) The generation of Langmuir circulations by an instability mechanism. *J. Fluid Mech.* **81,** 209–223.

Craik, A. D. D. (1982) The generalized Langrangian-mean equations and hydrodynamic stability. *J. Fluid Mech.* **125,** 27–35.

Craik, A. D. D. (1982) Wave-induced longitudinal-vortex instability in shear flows. *J. Fluid Mech.* **125,** 37–52.

Einstein, H. A. and Li, H. (1958) Secondary currents in straight channels. *Transactions, American Geographical Union* **39,** 1085–1088.

Hanratty, T. J. and Engen (1957) Interaction between a turbulent air stream and a moving water surface. *AIChE Journal* **3,** 299–304.

Langmuir, I. (1938) Surface motion of water induced by wind. *Science* **87,** 119–123.

Leibovich, S. and Ulrich, D. (1972) A note on the growth of small-scale Langmuir circulations. *Journal of Geophysical Research* **77,** 1683–1688.

Leibovich, S. (1977) On the evolution of the system of wind drift currents and Langmuir circulations in the ocean. Part 1: Theory and average current. *J. Fluid Mech.* **79,** 715–743.

Leibovich, S. and Radhakrishnan, K. (1977) On the evolution of the system of wind drift currents and Langmuir circulations in the ocean. Part 2: Structure of the Langmuir vortices. *J. Fluid Mech.* **80,** 481–507.

Leibovich, S. (1977) Convective instability of stably stratified water on the ocean. *J. Fluid Mech.* **82,** 561–585.

Leibovich, S. (1980) On wave-current interaction theories of Langmuir circulations. *J. Fluid Mech.* **99,** 715–724.

Leibovich, S. (1983) The form and dynamics of Langmuir circulations. *Ann. Rev. Fluid Mech.* **15,** 391–427.

Longuet-Higgins, M. S. (1953) Mass transport in water waves. *Phil. Trans. A* **245,** 535–581.

Magnaudet, J. (1989) Interactions interfaciales en écoulement à phases séparées. Thèse de Doctorat, Institut National Polytechnique de Toulouse.

Naot, D. and Rodi, W. (1982) Calculation of secondary currents in channel flow. *J. of the Hydraulics Division ASCE* **108,** 948–968.

Nezu, I. and Rodi, W. (1985) Experimental study on secondary currents in open channel flow. *Proc. of 21st IAHR Congress*, Melbourne, Vol. 2, pp. 115–119.

Nordsveen, M. and Bertelsen, A. F. (1993) Waves, turbulence and the mean field in stratified duct flow. Research Report in Mechanics, University of Oslo, ISBN 82-553-0837-7, No. 93-4.

Reynolds, W. C. and Husssain, A. K. M. F. (1972) The mechanics of an organized wave in turbulent shear flow. Part 3. Theoretical models and comparisons with experiments. *J. Fluid Mech.* **54,** 263–288.

Rodi, W. (1980) *Turbulence Models and Their Application in Hydraulics*. IAHR Book Publication, Delft, Netherlands.

Roston, H. I. and Spalding, D. B. (1987) The phoenics reference manual, CHAM TR/200.

Suzanne, C. (1985) Structure de l'ecoulement stratifie de gaz et de liquide en canal rectangulaire. Thèse de Docteur es Sciences. Institut National Polytechnique de Toulouse.

APPENDIX A

Mean Lagrangian to Mean Eulerian Momentum Equation

In section 2.3 we discussed the validation of the Taylor series expansion and linearization about the mean interface. It was argued that the effect of a thin oscillatory boundary layer at the interface could hardly be captured by such an approach. On the other hand the mean boundary layer was found thick enough to justify this approach. In this work we neglected the effect of the oscillatory boundary layer and apply Taylor series expansion and linearization about the mean interface.

A variant of theorem I in Andrews and McIntyre GLM theory (1978a), developed in section 2.1, reads

$$\underbrace{\bar{D}^{L}(\bar{\mathbf{v}}^{L}-\mathbf{P})+\nabla\bar{\mathbf{v}}^{L}\cdot(\bar{\mathbf{v}}^{L}-\mathbf{P})}_{\text{I}}=\underbrace{-\nabla\pi}_{\text{II}}-\underbrace{\bar{\mathbf{X}}^{L}}_{\text{III}}-\underbrace{\overline{\nabla\xi\cdot\mathbf{X}^{I}}}_{\text{III}}-\underbrace{\overline{\nabla(x-\xi)\cdot\nabla\cdot\langle\mathbf{v}'\mathbf{v}'\rangle}}_{\text{IV}}, \tag{54}$$

where π is given by

$$\pi=\frac{1}{\rho}\bar{p}^{L}-\frac{1}{2}\overline{\mathbf{v}^{\xi}\cdot\mathbf{v}^{\xi}}+\bar{\Phi}^{L}. \tag{55}$$

Term I. In the case studied, the mean Lagrangian velocity as well as the pseudomomentum are independent of time, and term I is readily shown to obey the relation

$$\underbrace{\bar{\mathbf{v}}^{L}\cdot\nabla(\bar{\mathbf{v}}^{L}-\mathbf{P})+\nabla\bar{\mathbf{v}}^{L}\cdot(\bar{\mathbf{v}}^{L}-\mathbf{P})}_{\text{I}}=\underbrace{-\bar{\mathbf{v}}^{L}\times\nabla\times(\bar{\mathbf{v}}^{L}-\mathbf{P})}_{\text{Ia}}+\underbrace{\nabla[\bar{\mathbf{v}}^{L}\cdot(\bar{\mathbf{v}}^{L}-\mathbf{P})]}_{\text{Ib}}. \tag{56}$$

The relation between the mean Lagrangian velocity, the mean Eulerian velocity and the Stokes drift is

$$\bar{\mathbf{v}}^{L}=\mathbf{V}+\bar{\mathbf{v}}^{S}. \tag{57}$$

Using this relation, term Ia may be transformed to

$$\mathbf{V}\cdot\nabla\mathbf{V}-\bar{\mathbf{v}}^{S}\times\nabla\times\mathbf{V}-(\mathbf{V}+\bar{\mathbf{v}}^{S})\times\nabla\times(\bar{\mathbf{v}}^{S}-\mathbf{P})-\underbrace{1/2\nabla(\mathbf{V}\cdot\mathbf{V})}_{\text{Ic}}. \tag{58}$$

The terms Ib and Ic are gradient terms and are included in term II.

Term II. With the above terms Ib and Ic, π becomes

$$\pi=\underbrace{\frac{1}{\rho}\bar{p}^{L}}_{\text{IIa}}-\underbrace{\frac{1}{2}\overline{\mathbf{v}^{\xi}\cdot\mathbf{v}^{\xi}}}_{\text{IIb}}-\underbrace{\frac{1}{2}\mathbf{V}\cdot\mathbf{V}}_{\text{IIc}}+\underbrace{\bar{\mathbf{v}}^{L}\cdot(\bar{\mathbf{v}}^{L}-\mathbf{P})}_{\text{IId}}+\underbrace{\bar{\Phi}^{L}}_{\text{IIe}}. \tag{59}$$

Assuming small displacements, a Taylor series expansion gives

$$\mathbf{v}^{\xi}=\mathbf{V}+\tilde{\mathbf{v}}+\xi\cdot\nabla\tilde{\mathbf{v}}+\frac{1}{2}\xi\xi:\nabla\nabla\mathbf{V}+O(|\xi|^{3}). \tag{60}$$

With this expression for $\mathbf{v}^{\xi}$, IIb can be expressed as

$$-\frac{1}{2}\overline{\mathbf{v}^{\xi}\cdot\mathbf{v}^{\xi}}=-\frac{1}{2}\mathbf{V}\cdot\mathbf{V}-\frac{1}{2}\overline{\tilde{\mathbf{v}}\cdot\tilde{\mathbf{v}}}-\mathbf{V}\cdot\bar{\mathbf{v}}^{S}. \tag{61}$$

The term IId is rearranged as

$$\bar{\mathbf{v}}^{L}\cdot(\bar{\mathbf{v}}^{L}-\mathbf{P})=\mathbf{V}\cdot\mathbf{V}+\mathbf{V}\cdot(\bar{\mathbf{v}}^{S}-\mathbf{P})+\bar{\mathbf{v}}^{S}\cdot\mathbf{V}. \tag{62}$$

It is now straightforward to rewrite π as

$$\pi=\frac{1}{\rho}\bar{p}^{L}-\frac{1}{2}\overline{\tilde{\mathbf{v}}\cdot\tilde{\mathbf{v}}}+\bar{\Phi}^{L}+\mathbf{V}\cdot(\bar{\mathbf{v}}^{S}-\mathbf{P}). \tag{63}$$

Term III. The flow studied is turbulent and we use wall functions to prescribe boundary conditions in the log-layer away from the walls where the viscous term is negligible. Accordingly term III is neglected.

Term IV. We introduce the following definitions:

$$\langle \mathbf{F} \rangle \equiv \nabla \cdot \langle \mathbf{v}'\mathbf{v}' \rangle, \tag{64}$$

$$\bar{\mathbf{F}} \equiv \overline{\nabla \cdot \mathbf{v}'\mathbf{v}'}, \tag{65}$$

$$\tilde{\mathbf{F}} \equiv \langle \mathbf{F} \rangle - \bar{\mathbf{F}}. \tag{66}$$

With these definitions, the term IV can be written

$$\overline{\nabla(\mathbf{x} + \xi) \cdot \langle \mathbf{F} \rangle}. \tag{67}$$

Inserting the Taylor series expansion of $\langle \mathbf{F}(\mathbf{x} + \xi, t) \rangle$ about $\mathbf{x}$

$$\langle \mathbf{F}(\mathbf{x} + \xi, t) \rangle = \langle \mathbf{F}(\mathbf{x}, t) \rangle + \nabla \langle \mathbf{F}(\mathbf{x}, t) \rangle \cdot \xi + O(|\xi|^2) \tag{68}$$

into [67] gives

$$\mathrm{IV} = \overline{\mathbf{F}(\mathbf{x}, t)} + \overline{\nabla \xi \cdot \tilde{\mathbf{F}}(\mathbf{x}, t)} + \overline{\xi \cdot \nabla \bar{\mathbf{F}}(\mathbf{x}, t)} + O(|\xi|^2), \tag{69}$$

where the relations $\bar{\bar{\mathbf{F}}} = \mathbf{0}$ and $\bar{\xi} = \mathbf{0}$ have been used. In this work the direct interaction between turbulence and waves has been neglected. That implies $\bar{\mathbf{F}} = \mathbf{0}$, and in accordance with this simplification only the first term is retained and IV becomes

$$\mathrm{IV} = \overline{\nabla \cdot \mathbf{v}'\mathbf{v}'}. \tag{70}$$

The mean Eulerian momentum equations are written as

$$\mathbf{V} \cdot \nabla \mathbf{V} = -\nabla \pi - \nabla \cdot \overline{\mathbf{v}'\mathbf{v}'} + \underbrace{\bar{\mathbf{v}}^{\mathrm{S}} \times \nabla \times \mathbf{V} + (\mathbf{V} + \bar{\mathbf{v}}^{\mathrm{S}}) \times \nabla \times (\bar{\mathbf{v}}^{\mathrm{S}} - \mathbf{P})}_{\bar{\mathbf{S}}}, \tag{71}$$

where

$$\pi = \frac{1}{\rho} \bar{p}^{\mathrm{L}} - \frac{1}{2} \overline{\tilde{\mathbf{v}} \cdot \tilde{\mathbf{v}}} + \bar{\Phi}^{\mathrm{L}} + \mathbf{V} \cdot (\bar{\mathbf{v}}^{\mathrm{S}} - \mathbf{P}). \tag{72}$$

APPENDIX B

The Displacement Field

From a given perturbation velocity field the corresponding displacements are developed. This was done by Craik (1982a) for one plane wave (Fourier component) disturbing a unidirectional mean shear flow. The wave field with the interfacial model B in section 2.2 is the same as the one Craik used. The corresponding displacements for this case are presented below and we refer to Craik (1982a) for more details. In the interfacial model A the interface deformation was composed of two crossing plane waves. We show the development of the displacements for this wave field.

Interfacial model B

A unidirectional, $O(1)$ shear flow $[0, 0, \hat{W}(y)]$ is perturbed by an $O(\epsilon_1)$ wave disturbance given by

$$\tilde{u} = 0, \tag{73}$$

$$\tilde{v} = \epsilon_1 \mathrm{real}[\phi_y(y) \mathrm{e}^{ik_w(z - ct)}], \tag{74}$$

$$\tilde{w} = \epsilon_1 \mathrm{real}[-i\phi_z(y) \mathrm{e}^{ik_w(z - ct)}], \tag{75}$$

where

$$\phi_z(y) = -\phi_{yy}/k_w. \tag{76}$$

The displacements were given by Craik (1982, [3.2]) and read

$$\xi_x = 0, \tag{77}$$

$$\xi_y = \frac{\phi_y(y)}{k_w(\hat{W} - c)} \sin[k_w(z - ct)] + O(\epsilon_1^2), \tag{78}$$

$$\xi_z = -\left(\frac{\hat{W}_y \phi_y(y)}{k_w(\hat{W} - c)} + \phi_z(y)\right) \frac{1}{k_w(\hat{W} - c)} \cos[k_w(z - ct)] + O(\epsilon_1^2). \tag{79}$$

Interfacial model A

A unidirectional, $O(1)$ shear flow $[0, 0, \hat{W}(y)]$ is perturbed by an $O(\epsilon_1)$ wave disturbance given by

$$\tilde{u} = \epsilon_1 \text{real}[2\phi_x(y)\cos \beta x e^{i\alpha(z - ct)} e^{\sigma t}], \tag{80}$$

$$\tilde{v} = \epsilon_1 \text{real}[2\phi_y(y)\sin \beta x e^{i\alpha(z - ct)} e^{\sigma t}], \tag{81}$$

$$\tilde{w} = \epsilon_1 \text{real}[-i2\phi_z(y)\sin \beta x e^{i\alpha(z - ct)} e^{\sigma t}], \tag{82}$$

where $\phi_x(y)$ and $\phi_z(y)$ are given by

$$\phi_x(y) = \frac{\beta}{k_w^2}\left(\phi_{y,y} - \frac{\phi_y \hat{W}_y}{\hat{W} - c}\right), \tag{83}$$

$$\phi_z(y) = -\frac{\alpha}{k_w^2}\left(\phi_{y,y} + \frac{\beta^2}{\alpha^2} \frac{\phi_y \hat{W}_y}{\hat{W} - c}\right). \tag{84}$$

The velocity field is temporarily multiplied with the exponential growth term $e^{\sigma t}$. A fluid particle in the position (X_0, Y_0, Z_0) at some initial time t_0 has the position (X, Y, Z) for $t > t_0$ given by

$$X(t) = X_0 + \int_{t_0}^{t} u[X(s), Y(s), Z(s)]\mathrm{d}s, \tag{85}$$

$$Y(t) = Y_0 + \int_{t_0}^{t} v[X(s), Y(s), Z(s)]\mathrm{d}s, \tag{86}$$

$$Z(t) = Z_0 + \int_{t_0}^{t} w[X(s), Y(s), Z(s)]\mathrm{d}s, \tag{87}$$

where u, v and w are the velocity components. To $O(1)$ only the mean axial flow exists and we obtain

$$X(t) = X_0, \tag{88}$$

$$Y(t) = Y_0, \tag{89}$$

$$Z(t) = Z_0 + \hat{W}(y)(t - t_0). \tag{90}$$

To $O(\epsilon_1)$ also the wave perturbation velocity components contribute to the position (X, Y, Z). The derivation of the $X(t)$ coordinate will be given in some detail.

$$X(t) = X_0 + \epsilon_1 \text{real}\left[\int_{t_0}^{t} 2\phi_x(Y_0)\cos\beta X_0 e^{i\alpha(Z_0 + \hat{W}(s-t_0) - cs)} e^{\sigma s} ds\right] \quad [91]$$

$$= X_0 + \epsilon_1 \text{real}\left[\frac{2\phi_x(Y_0)\cos\beta X_0}{i\alpha(\hat{W} - c) + \sigma} e^{i\alpha(Z_0 - \hat{W}t_0)}(I\text{–}II)\right] \quad [92]$$

$$I = e^{[i\alpha(\hat{W} - c) + \sigma]t} \quad [93]$$

$$II = e^{[i\alpha(\hat{W} - c) + \sigma]t_0}. \quad [94]$$

The perturbation is assumed to grow initially from zero to a small $O(\epsilon_1)$ value, when $\sigma \to 0$. That is, we put $\sigma = 0$ in I. In addition we choose $t_0 = -\infty$ which gives $II = 0$. $X(t)$ is then given by

$$X(t) = X_0 + \epsilon_1 \text{real}\left[\frac{2\phi_x(Y_0)\cos\beta X_0}{i\alpha(\hat{W} - c)} e^{i\alpha(Z - ct)}\right]. \quad [95]$$

Similarly, one finds that $Y(t)$ is given by

$$Y(t) = Y_0 + \epsilon_1 \text{real}\left[\frac{2\phi_y(Y_0)\sin\beta X_0}{i\alpha(\hat{W} - c)} e^{i\alpha(Z - ct)}\right]. \quad [96]$$

To $O(\epsilon_1)$ there will be an extra contribution from the primary flow to the $Z(t)$ coordinate. A Taylor series expansion of $\hat{W}(Y)$ about Y_0 reads

$$\hat{W}(Y) = \hat{W}(Y_0) + \hat{W}_{,y}(Y_0)\epsilon_1 \text{real}\left[\frac{2\phi_y(Y_0)\sin\beta X_0}{i\alpha(\hat{W} - c) + \sigma} e^{i\alpha(Z - ct)} e^{\sigma t}\right] + O(\epsilon_1)^2, \quad [97]$$

where σ is still retained. The $Z(t)$ coordinate is now found to be

$$Z(t) = Z_0 + \hat{W}(Y_0)(t - t_0) + \epsilon_1 \text{real}\left[\left(\frac{\hat{W}_{,y}(Y_0)2\phi_y(Y_0)}{i\alpha(\hat{W} - c)} - i2\phi_z(Y_0)\right)\frac{\sin\beta X_0}{i\alpha(\hat{W} - c)} e^{i\alpha(z - ct)}\right]. \quad [98]$$

The displacements to $O(\epsilon_1)$ are hence given by

$$\xi_x = 2\epsilon_1 \text{real}\left[\frac{\phi_x(y)\cos\beta x}{i\alpha(\hat{W} - c)} e^{i\alpha(z - ct)}\right], \quad [99]$$

$$\xi_y = 2\epsilon_1 \text{real}\left[\frac{\phi_y(y)\sin\beta x}{i\alpha(\hat{W} - c)} e^{i\alpha(z - ct)}\right], \quad [100]$$

$$\xi_z = 2\epsilon_1 \text{real}\left[\left(\frac{\hat{W}_{,y}\phi_y(y)}{i\alpha(\hat{W} - c)} - i\phi_z(y)\right)\frac{\sin\beta x}{i\alpha(\hat{W} - c)} e^{i\alpha(z - ct)}\right]. \quad [101]$$

Note the change from X_0 to x, Y_0 to y and $Z_0 + \hat{W}(Y_0)(t - t_0)$ to z in accordance with the GLM description.